BAU Journal - Science and Technology

Volume 4 | Issue 1
ISSN: 2706-784X

Article 9

December 2022

STRUCTURAL AND MAGNETO CONDUCTIVITY STUDIES OF NIO/ SMBA2CU3O7-Δ SUPERCONDUCTING COMPOSITE

Hadi Basma
Department of Physics, Faculty of Science, Beirut Arab University, h.basma@bau.edu.lb

Sajida Rmeid
Department of Physics, Faculty of Science, Beirut Arab University, smr410@student.bau.edu.lb

Ramadan Awad
Department of Physics, Faculty of Science, Beirut Arab University,Department of Physics, Faculty of Science, Alexandria University, ramadan.awad@bau.edu.lb

Mohammed Said
Department of Physics, Faculty of Science, Alexandria University, mohammedscience2013@alex.edu.eg

1. INTRODUCTION

Since their discovery, $SmBa_2Cu_3O_{7-\delta}$ (Sm-123) high-temperature superconductors have grabbed the attention of researchers due to several favorable properties that allow for significant applications (Wang et al., 2021). Sm-123 superconductors are characterized by a high ability to trap large magnetic fields and hence carry a substantial critical current density (Wang et al., 2021). Owing to these properties, Sm-123 superconductors have found applications in various fields such as transmission cables, motors, and magnetic energy storage systems (Najjar et al., 2020).

Furthermore, Sm-123 superconductors are characterized by a short coherence (2-4 nm) at temperatures below 77K (Abdeen et al., 2016). This means that the addition of a secondary phase to the superconducting matrix might serve as an effective pinning center. These pinning centers prevent thermally activated flux creep and hence allow achieving higher J_c values. Several pieces of research have explored the effect of magnetic and nonmagnetic nanoparticles' addition on Re-123 (Rmeid et al., 2019, Barakat , 2017, Abdeen et al., 2016, Awad et al., 2015, Basma et al., 2016, Basma et al., 2015). Most studies have shown that small amounts of Nano addition cause an enhancement of the superconducting parameters while higher amounts lead to deterioration.

On the other hand, the investigation of the transport properties of HTSC is crucial for the understanding of the effect of the nano additions. The analysis of the electric resistivity and the magneto conductivity can contribute significantly to this understanding (Nasser et al., 2020, Khadzhai et al., 2021). For instance, El-Said Bakeer et al. (Abdeen et al., 2016) studied the effect of $CoFe_2O_4$ addition on the Gd-123 system. The magneto conductivity analysis showed a strong correlation between the amount of added $Cofe_2O_4$ and the superconductivity parameters. Moreover, Aftabi and Mozaffari (Aftabi et al., 2021) explored the effect of nano ZnO addition on (Bi,Pb)2223 superconducting phase. The values of the upper and lower critical magnetic fields and the critical current densities and the coherence lengths were enhanced as a result of the addition of 0.2 wt% of ZnO. The enhancement of the critical parameters was attributed to the pinning of magnetic vortices and the enhancement of intergranular coupling induced by the addition of NiO nanoparticles.

NiO nanoparticles have recently attracted the focus of researchers in various domains, such as supercapacitors, photovoltaic cells, gas sensors, photocatalytic devices, and biosensors (Abdallah Basma et al., 2019, Sery et al., 2022, Sankar Basma et al., 2022, Sun et al., 2021).

Furthermore, the addition of NiO to high-temperature superconductors has shown promising results in terms of enhancing their transport properties (Rahal et al., 2018, Awad et al., 2019, Zhao et al., 2021)To the best of our knowledge, the effect of NiO nanoparticles' addition on the superconducting properties of the Sm-123 system has not been investigated before. Thus, we aim to explore the effect of the addition of the nanoparticles on the crystal structure and transport properties of the Sm-123 superconducting system by preparing six samples of $(NiO)_xSmBa_2Cu_3O_{7-\delta}$, $0.00 \leq x \leq 0.12$ wt.%, using the conventional solid-state reaction. The crystal structure and morphology of the samples are investigated using XRD powder diffraction, and SEM imaging, respectively. The dc-electrical resistivity measurements were performed in the absence and presence of a magnetic field. The results are analyzed based on the effect of added NiO.

2. EXPERIMENTAL TECHNIQUES

The NiO nanoparticles were prepared by the chemical coprecipitation method, while the Sm-123 superconducting system was prepared by the conventional solid-state reaction technique reported elsewhere (Rmeid et al., 2019). The crystal structure was explored using a Bruker D8 Advance powder diffractometer. The spectra were recorded at room temperature with Cu–Kα radiation ($\lambda = 1.54056$ Å) and 2θ ranging from 5 to 80º. scanning electron microscopy (SEM) was applied to identify the surface morphology and grain connectivity of the samples using a Jeol scanning electron microscope JSM-5300, operated at 25 kV, with a resolution power of 4 nm and a magnification range of 7500. Electric resistivity measurements were performed using the standard four-probe technique for the prepared samples. The working medium represents a closed cryogenic refrigeration system using liquid nitrogen as a coolant; the results were carried out with the variation of temperature from room temperature down to lower ones ($77\ K \leq T \leq \sim 300\ K$),

allowing to determine *T*c and zero superconducting transition temperature (T_0). An Fe–Au thermocouple was used to monitor the temperature of the sample which can be stabilized through the aid of a temperature controller to within ±0.1 K. The measurements of electrical resistivity versus temperature were also performed at an applied dc magnetic field of 0.44 T. The magnetic field was generated from a dc electromagnet and applied normally to the direction of the driving current.

3. RESULTS AND DISCUSSIONS

3.1 XRD Analysis:

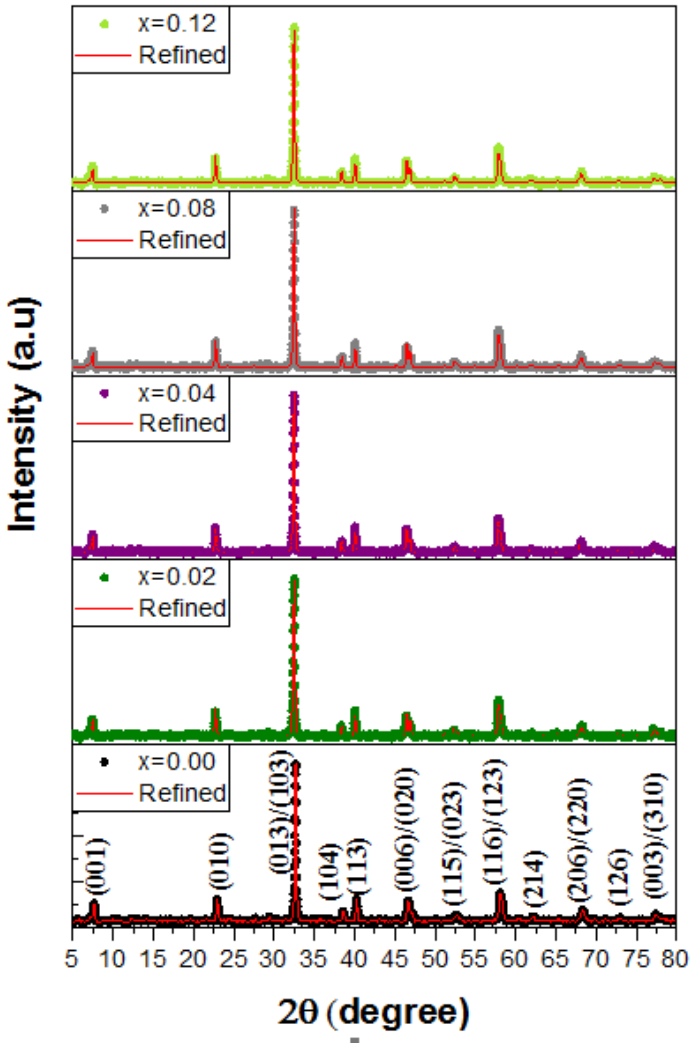

Fig.1: XRD-patterns with Reitveld refinements for $(NiO)_xSmBa_2Cu_3O_{7-\delta}$ (x =0.00, 0.02,0.04, 0.08 and 0.12 wt %).

Table 1 Lattice parameters, orthorhombic distortion and oxygen content of $(NiO)_x$/ $SmBa_2Cu_3O_{7-\delta}$ (x=0.00, 0.02,0.04, 0.08 and 0.12 wt. %)

x	a(Å)	b((Å)	c(Å)	Od(%)
0.00	3.877	3.905	11.715	0.359
0.02	3.871	3.906	11.723	0.450
0.04	3.875	3.907	11.711	0.411
0.08	3.872	3.906	11.704	0.437
0.12	3.873	3.904	11.717	0.398

The graphs of figure 1 show the XRD patterns of $(NiO)_x SmBa_2Cu_3O_{7-\delta}$ (x=0.00, 0.02,0.04, 0.08 and 0.12 wt %) with their Reitveld refinements performed with the aid of the MAUD software (Lutterotti, 2000). The formation of superconducting samples of high purity and crystallinity is confirmed. All diffraction peaks of the pattern match the orthorhombic structure of space group pmmm JCPDS card No. 89-8900 (Wang et al., 2017). The XRD pattern shows the absence of peaks corresponding to nanosized particles NiO. Moreover, the 2-θ positions of all diffraction peaks show no shift with the addition of the NiO nanoparticles. These observations infer that the nanosized particles did not enter inside the crystal structure and stayed as adhering materials on the surface and grain boundaries. The lattice parameters a, b and c, were determined by applying a Reitveld refinement using the MAUD software, and are listed in Table1. The values of the lattice parameters show an unsystematic variation with the addition of nanosized particles close to those of the pure sample. This result supports the claim that the nanosized particles NiO do not enter inside the crystal structure of Sm-123, but resides at the grain boundaries. Similar results were obtained by Abdeen. et al. (Abdeen et al., 2016) in $SmBa_2Cu_3O_{7-\delta}$ superconductor phase added with nanosized particles $MnFe_2O_4$ and by Basma et al. (Basma et al., 2016) for $GdBa_2Cu_3O_{7-\delta}$ superconductor phase added with nanosized $CoFe_2O_4$.The orthorhombic distortion is also calculated by using equation (1) (Awana et al., 2021)

$$O_d(\%) = \left[\frac{b-a}{b+a}\right] * 100 \qquad (1)$$

and the values are displayed in table 1. The values of Od do not show a systematic variation with the addition of the NiO, consistent with the variation of the lattice parameters a and b. However, the low values of Od (Od < 1%) confirm the stability of the orthorhombic phase with the addition of the NiO nanoparticles. It should be noted that the crystallographic splitting of (110)/ (103), (006)/ (020), and (116)/ (123) diffraction planes of the XRD patterns also shows evidence of no orthorhombic to tetragonal (O–T) phase transition

3.2 SEM Images

The Micrographs of Figures 2(a-d) show the SEM images of $(NiO)_x$ $SmBa_2Cu_3O_{7-\delta}$ samples (x=0.00, 0.02, 0.04 and 0.12 wt %)**.** The morphological examination of the pure sample (Figure 2-a) displays well-connected grains with random orientations. The size of the grains ranged between 0.72μm to 1.6μm without a systematic variation upon the addition of the nanoaprticles.Upon the addition of NiO nanoparticles, (figure 2-b) similar grains morphology appears with randomly distributed globules and patches, due to the accumulation of nanosized particles NiO on the surface. For higher additions of nanosized particles NiO figures (2-c and 2-d), tiny white particles appear in the same range within the rectangular grains. This may be due to the adhesion of nanosized particles (NiO) to the surface of the grains, leading to a more uniform surface appearance and good connectivity between grains compared to the pure sample.

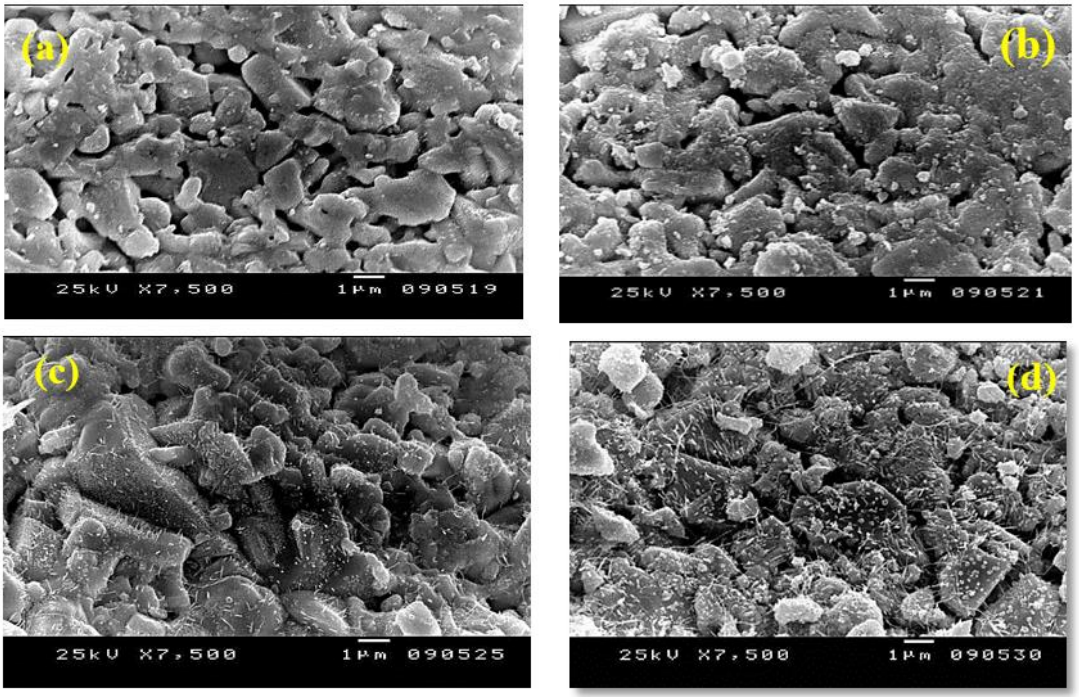

Fig.2(a-d): SEM images for $(NiO)_x\ SmBa_2Cu_3O_{7-\delta}$ samples (x=0.00, 0.02, 0.04 and 0.12 wt %, respectively).

3.3 Electrical Resistivity Measurements:

The temperature dependence of the electrical resistivity for $(NiO)_x\ SmBa_2Cu_3O_{7-\delta}$ with x = 0.00, 0.02, 0.04,0.08 and 0.12wt% is shown in the plots of figure 3. All the samples show a metallic-like behavior in the normal state followed by a superconducting transition at T_c, and zero resistivity at temperature T_0. The small curvature that appears above T_c characterizes the fluctuations of the cooper pairs *(Basma et al., 2015).*

The fitting of the normal state resistivity data is done using Matthiessen's rule (White et al., 1986), as shown in equation (2)

$$\rho = \rho_0 + \alpha T, \qquad (2)$$

Where ρ_0 represents the residual resistivity and α represents the resistivity coefficient α. The values of ρ_0 and α are listed in table.3, in addition to the normal state resistivity ρ_{room}. It is well known that ρ_{room} is an indicator for the disorder of cations and oxygen vacancies which increase the number of scattering centers (White et al., 1986) and ρ_0 is an indicator for the purity of the sample. It is clear that both ρ_{room} of $(NiO)_x\ SmBa_2Cu_3O_{7-\delta}$ decrease with the increase of nanosized NiO addition from x = 0.00 to x = 0.04 wt% and then increase for x > 0.04 wt%. The decrease in ρ_{room} is an indication of the reduction of the grain boundaries and defects and the improvement in the quality and purity of the samples. Whereas the strong increase of ρ_{room} and ρ_o for x >0.04 may be strongly related to the impurities and scattering of grain boundaries. The increase in α with x >0.04 for $(NiO)_x\ SmBa_2Cu_3O_{7-\delta}$ could be due to the unsuspected temperature-dependent scattering (magnetic impurities scattering) contribution by nanosized NiO (Abou-Aly, et al., 2009)

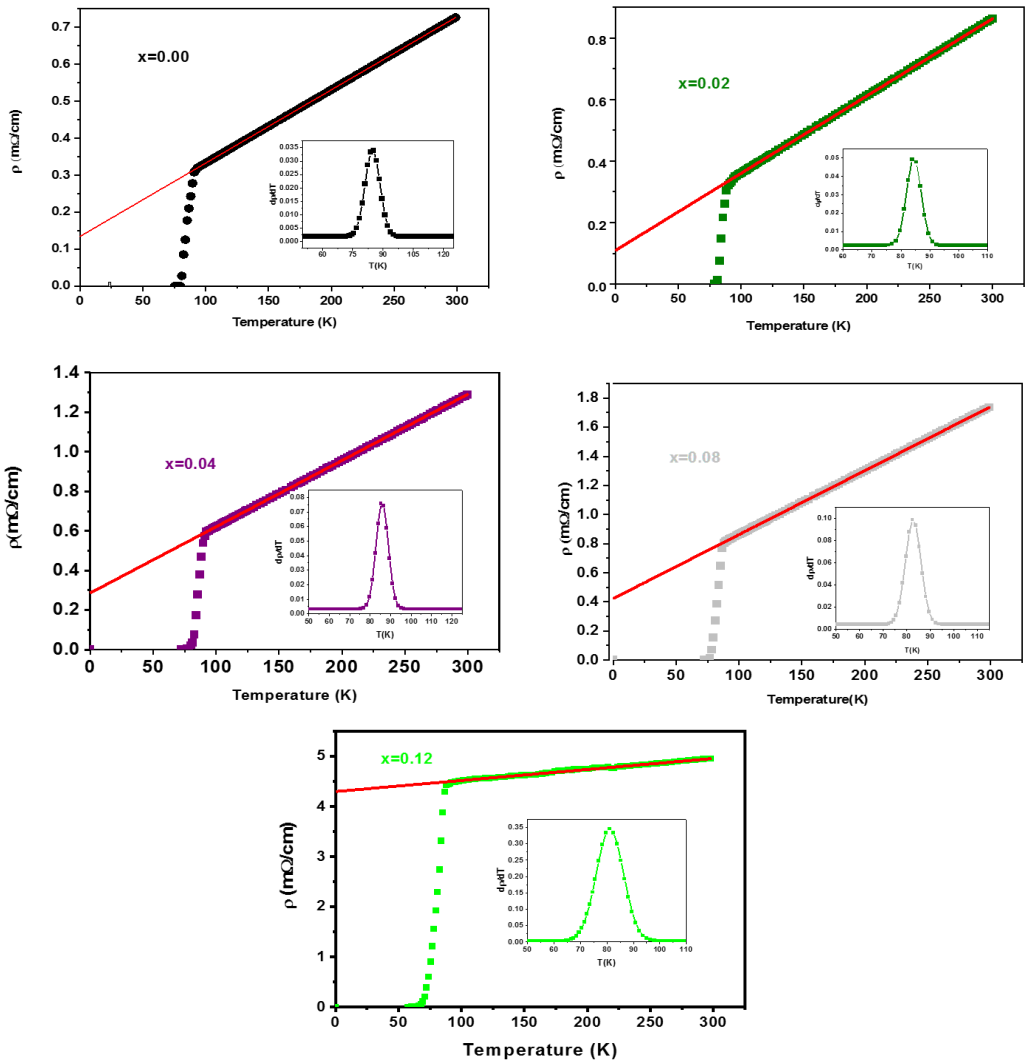

Fig.3: The variation of electric resistivity ρ versus temperature for $(NiO)_xSmBa_2Cu_3O_{7-\delta}$ ($0.00 \leq x \leq 0.12$ wt.%). The inset shows dρ/dt with temperature.

The superconducting transition temperature T_c, which displays the superconducting transition within the grains, is determined as the temperature corresponding to the crest in $d\rho/dT$ curve (Salamati et al., 2003). The derivative of $\rho(T)$ versus T curves for $(NiO)_xSmBa_2Cu_3O_{7-\delta}$ with x = 0.0, 0.02, 0.04, 0.08, 0.12wt.% are shown in the insets of the plots of figure 3. All the samples show a single peak at *Tc*, indicating the transition within the superconducting grains. The values of T_c, T_0, and ΔT for $(NiO)_xSmBa_2Cu_3O_{7-\delta}$ are listed in Table 3. The value of T_c for $SmBa_2Cu_3O_{7-\delta}$ is 84.753 K very close to the that reported in the literature (Wen et al., 1992). It is obvious that T_c for $(NiO)_x$ $SmBa_2Cu_3O_{7-\delta}$ increasesfrom 84.7533K to 86.328K as x varies from 0.00 to 0.04 wt%, then it decreases for x > 0.04 wt%. The increase of T_c with x could be explained due to the improvement in the intergrain connectivity induced by the addition of the NO nanoparticles. Whereas, the suppression of T_c for higher NiO additions, may be strongly related to, pair-breaking, the trapping of mobile free carriers (Qasim et al., 2016, Khan et al., 2010, Elmustafa et al., 2003), and the non-uniform distribution of NiO nanoparticles on the superconductor surface. This behavior can be interpreted as a result of the magnetic role of NiO nanosized, which would affect the long-range coupling of Cu ion in the CuO layer and cancel the supercurrents. This result is consistent with the known behavior of the bulk superconductors added with small amounts of magnetic impurities (Javed et al., 2016).

T_0 characterizes the onset of global superconductivity (where all grains become superconducting i.e. intragrain as well as grain boundaries become superconducting) in the samples where the long-range superconducting order is achieved. As seen from Table 3 , T_0

for $(NiO)_xSmBa_2Cu_3O_{7-\delta}$ increases from 79.688 K to 81.329 K as x varies from0.00 to 0.04wt%, then it decreases for x > 0.04wt%. The decrease in T_0 with x is attributed to the progressive of microscopic inhomogeneities such as grain boundaries and twin boundaries in the bulk(Javed et al., 2016). The superconducting transition width ΔT was calculated to examine the purity of the prepared samples. The decrease in ΔT with x up to 0.04 is related to the improvement of the homogeneity of the superconducting sample due to the addition of the NiO nanoparticles. The further increase in ΔT is due to the presence of macroscopic inhomogeneities induced by the presence of the NiO addition.

Table 2 T_c, T_0, ΔT, ρ_0, ρ_{room}, and α versus x wt% for $(NiO)_x SmBa_2Cu_3O_{7-\delta}$

NiO (wt %)	T_c (K)	T_0 (K)	ΔT(K)	ρ_{room}(Ω.cm)	ρ_0(Ω.cm)	α (Ω.m.k^{-1})
0.00	84.753	79.688	5.065	1.826	0.134	0.0019
0.02	85.669	80.000	5.669	1.762	0.109	0.0025
0.04	86.328	81.329	4.995	1.289	0.287	0.0034
0.08	82.799	73.950	10.849	1.735	0.423	0.0044
0.12	81.772	60.690	21.082	4.947	4.298	0.0022

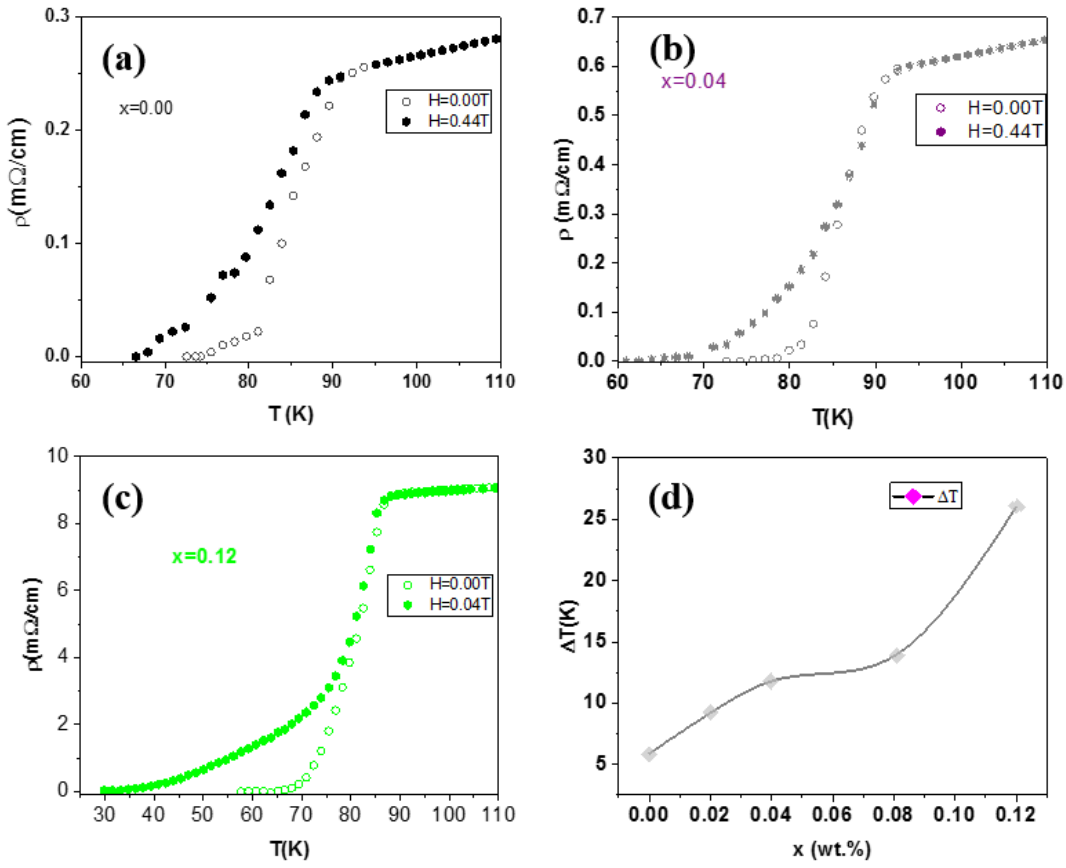

Fig.4 (a-c): Variation of the electrical resistivity versus temperature at zero and applied magnetic field of 0.44 T for samples with x=0.00, 0.04, and 0.12 wt.%.

Fig.4(d): Variation of ΔT_0 versus NiO-content for $(NiO)_xSmBa_2Cu_3O_{7-\delta}$ samples with $0.00 \leq x \leq 0.12$.

The plots of fig.3, show the variation of the resistivity of the samples x=0.00, x=0.04, and x=0.12 versus temperature at H=0.00T and H=0.04T. All graphs show a negligible effect of the magnetic field in the normal state (above T_c). However, a small shift in the value of T_c appears as a result of applying the external magnetic field. This is attributed to the presence of strong intragrain pinning energy. This energy forbids the motion of vortices near the

superconducting transition temperature region (Awad et al., 2001). For T< T_c, the dependence of the resistivity on the magnetic field becomes more evident. A tail in the resistivity curve appears as a result of the weak links between the grains. For higher additions of NiO (x=0.04 and x=0.12), the resistivity curve becomes broader and shifts to lower temperatures. This is revealed in the plot of figure 4-d, which shows the variation of transition width $\Delta T_0=T_0(0)-T_0(B)$, where $T_0(0)$ is the resistivity in the absence of an applied magnetic field and $T_0(B)$ is the resistivity in the presence of the magnetic field. The values of ΔT_0 are also listed in table 3. The broadening of the transition width is a measure of the strength of the pinning force (Mohammadizadeh et al., 2003). The addition of the NiO nanoparticles has significantly increased the pinning force. The increase in the transition width is attributed to several factors including the oxygen content, quality of the intergrain weak links, and the homogeneity of grains.

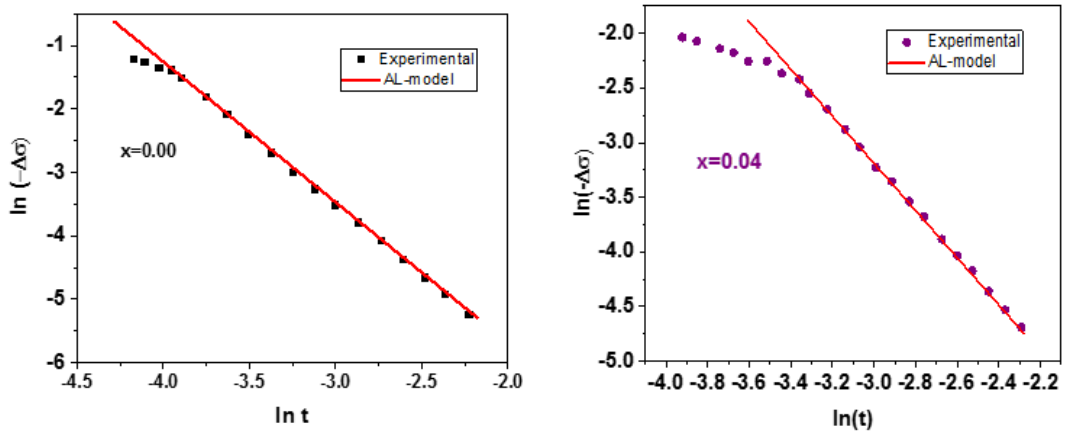

Fig.5: Variation of ln$(-\sigma H)$ versus ln t $(NiO)_x$ $SmBa_2Cu_3O_{7-\delta}$ with x = 0.0 (a) and 0.04 wt.% (b).

Table 3 Parameters obtained from magnetic conductivity analysis for $(NiO)_x$ $SmBa_2Cu_3O_{7-\delta}$

NiO (wt %)	ΔT_0	$\xi_c(0)$ (Å)	$\xi_{ab}(0)$ (Å)	Γ
0.00	6.7	9.52	53.37	5.61
0.02	9.2	8.32	61.25	7.36
0.04	12.3	28.61	210.72	7.36
0.08	14.5	21.41	208.12	9.812
0.12	26.8	17.62	198.23	11.2

The experimental magneto-conductivity, $\Delta\sigma_B$, is calculated according to the relation:

$$\Delta\sigma_B = \left(\frac{1}{\rho(B)}\right) - \left(\frac{1}{\rho(0)}\right) \qquad (3)$$

where $\rho(B)$ represents the experimental resistivity under the applied magnetic field, while $\rho(0)$ represents the experimental resistivity in the absence and presence of the magnetic field.

The plots of figures 5(a-b) show the logarithmic plots of $(-\Delta\sigma_B)$ versus the reduced temperature t given by $t = \frac{T-T_c}{T_c}$, for the samples having x=0.00 and x=0.04. The fitting obtained by employing the AL- model is also shown in the plots.

The expression for the magneto - conductivity due to the orbital contribution on (AL) term, $\Delta\sigma_{ALO}$ is given according to the Aslamazov–Larkin (AL) (Hikami et al., 1988)model by

$$\Delta\sigma_{ALO} = \frac{-e^2}{64\hbar d_e t^3}\frac{2+4\alpha+3\alpha^2}{(1+2\alpha)^{5/2}}\mathrm{H}^2 \qquad (4)$$

where, $\alpha = \alpha_0/t = \left(2\xi_c(0)^2/d_e{}^2\right)/t$, d_e is the effective layer thickness, and $\mathrm{H}^2 = H_{eff}{}^2(2e\xi_{ab}(0)^2/\hbar)^2$, with H_{eff} being the effective magnetic field.

For a polycrystalline sample, according to Matsuda et al. (Matsuda et al., 1988), the effective magnetic field is given by $H_{eff}{}^2 = H^2\langle\cos^2\Theta\rangle = H^2/3$, where H is the applied magnetic field and Θ is the angle between H and the c direction of the crystallite. The fitting was done according to equation (4) by varying the parameters α_0, $s = (e^2/64\hbar d)$. The resulting fitting parameters allowed to calculate $\xi_c(0)$, $\xi_{ab}(0)$ and $\Gamma = \xi_{ab}/\xi_c$. The results are depicted in table 3. The results indicated that the values of both coherence lengths for the pure sample are comparable to those reported in previous literature (Barakat , 2017, Abdeen et al., 2016).The short coherence length in the order of a few Å is a characteristic of high-temperature superconductors. It is attributed to the existence of overlapping energy bands (Aftabi et al., 2021,Habanjar et al., 2019). Upon the addition of NiO both $\xi c(0)$ and $\xi ab(0)$ increase with x up to 0.04 and then decrease with further increase in x. The simple grain model (Aftabi et al., 2021)serves to interpret the findings. According to this model, the transport behavior in ceramic structures depends on several factors including the mixing of the insulting c axis with the conducting (ab) planes, on the inhomogeneities and defects within the crystal structure as well as on the boundaries of the crystal.

The observed increase of the coherence length over several electronic layers along the *c*-axis, up to *x* = 0.12 wt.%, gives rise to an increased coherence volume containing Cooper pairs formed at higher temperatures and results in an increase of T_c. The further decrease in the coherence length reflects the decrease in the density of charge carriers in conducting planes (Almessiere et al., 2020, Phys, 2014). This might be because the large content of added magnetic NiO nanoparticles hinders the transport properties by increasing the resistance to the tunneling of the carriers through the grain boundaries.

The value of the anisotropy parameter of the pure sample is comparable to that of the Gd-123 system having a similar crystal structure (Lundqvist et al., 2000). The values of Γ increase with the increase of the addition of NiO nanoparticles as a result of the increase of the coherence length along the ab plane.

4. CONCLUSION

The solid-state reaction method was employed to prepare a series of $NiO_x/SmBa_2Cu_3O_{7-\delta}$ superconducting composites with $0.00 \le x \le 0.12$. The XRD analysis showed no variation in the orthorhombic structure of the superconducting matrix and unsystematic variations of the lattice parameters. This in addition to the morphological examination of the samples using, suggested the residing of the NiO nanoparticles at the level of the grain boundaries. The superconducting transition temperature, as obtained from electrical resistivity measurements was enhanced with the addition of NiO up to x=0.04, followed by a further decrease.

Moreover, the magneto-conductivity analysis was formed under an external applied Dc Field H=0.44T. A strong dependence of the resistivity on the applied field below T_c was observed, with a remarkable increase in the transition width. This suggests an enhancement of the pinning force as a result of the addition of the NiO nanoparticles. The AL- model was employed to analyze

the magneto conductivity versus the reduced temperature. The variations of the coherence lengths and the anisotropy parameter were correlated to the variations of the superconducting parameters.

ACKNOWLEDGMENTS

This research was accomplished in the Specialized Materials Science Lab and Advanced Nanomaterials Research Lab, Physics Department, Faculty of Science, Beirut Arab University, Lebanon in collaboration with the superconductivity and metallic-glass lab, Faculty of Science, Alexandria University, EGYPT.

This research did not receive any specific grant from funding agencies in the public, commercial, or not-for-profit sectors.

REFERENCES

- Abdeen, W., El-Tahan, A., Roumié, M., Awad, R., Abou Aly, A. I., El-Maghraby, E. M., & Khalaf, A. (2016). Role of improving the physical properties of Sm-123 phase by adding nano-magnetic $MnFe_2O_4$. *Journal of Magnetism and Magnetic Materials*, *419*, 354-362.
- Abdeen, W., El Tahan, A., Awad, R., Abou Aly, A. I., El-Maghraby, E. M., & Khalaf, A. (2016). Superconductivity and mechanical properties of $SmBa_2Cu_3O_{7-\delta}$ added with nano-crystalline $ZnFe_2O_4$. *Applied Physics A*, *122*(6), 574.
- Abdallah, A. M., Basma, H., & Awad, R. (2019). Preparation, characterization, and application of nickel oxide nanoparticles in glucose and lactose biosensors. *Modern Applied Science*, *13*(6), p99.
- Aftabi, A., & Mozaffari, M. (2021). Fluctuation induced conductivity and pseudogap state studies of $Bi_{1.6}Pb_{0.4}Sr_2Ca_2Cu_3O_{10+\delta}$ superconductor added with ZnO nanoparticles. *Scientific reports*, *11*(1), 1-15.
- Abou-Aly, A. I., Awad, R., Ibrahim, I. H., & Abdeen, W. (2009). Excess conductivity analysis for $Tl_{0.8}Hg_{0.2}Ba_2Ca_2Cu_3O_{9-\delta}$ substituted by Sm and Yb. *Solid State Communications*; *149*(7-8), 281-285.
- Almessiere, M. A. et al. Dimensionality and superconducting parameters of $YBa_2Cu_3O_{7-d}/(WO_3NPS)_x$ composites deduced from excess conductivity analysis. Mater. Chem. Phys. 243, 122665 (2020).
- Awad, R., Roumié, M., Isber, S., Marhaba, S., AbouAly, A. I., & Basma, H. (2015). Investigation of Temperature Dependence of the Irreversibility Line of $GdBa_2Cu_3O_{7-\delta}$ Added with Nanosized Ferrite $ZnFe_2O_4$. *Journal of Superconductivity and Novel Magnetism*, *28*(2), 535-539.
- Awad, R., Rahal, H. T., Abdel-Gaber, A. M., & Abou-Aly, A. I. (2019). Excess Conductivity and Magnetoconductivity Analysis of $(NiO)_x$(Bi,Pb)-2223 Superconducting Phase. *Journal of Superconductivity and Novel Magnetism*, *32*(9), 2733-2737.
- Awad, R., Aly,N.S., Ibrahim, I.H. , Abou-Aly, A.I., Saad, A.I., Physica B **307**, 72 (2001).
- Awana, V. P. S., Malik, S. K., & Yelon, W. B. (1996). Structural aspects and superconductivity in oxygen-deficient $Y_{1-x}Ca_xBa_2Cu_3O_{7-y}$ ($y \approx 0.3$) system A neutron-diffraction study. *Physica C: Superconductivity*, *262*(3-4), 272-278.
- Barakat, M. M. (2017). Role of ruthenium content in studying excess conductivity and magneto-conductivity of $SmBa_2Cu_{3-x}Ru_xO_{7-\delta}$ phase. *Journal of Materials Science: Materials in Electronics*, *28*(18), 13912-13919.
- Basma, H., Awad, R., Roumié, M., Isber, S., Marhaba, S., & AbouAly, A. I. (2016). Study of the Irreversibility Line of $GdBa_2Cu_3O_{7-\delta}$ Added with Nanosized Ferrite $CoFe_2O_4$. *Journal of Superconductivity and Novel Magnetism*, *29*(1), 179-185.
- Basma, H., Roumié, M., Awad, R., Marhaba, S., Albast, M., & Abualy, A. (2015). Ion beam analysis and electric properties of $GdBa_2Cu_3O_{7-\delta}$ added with nanosized ferrites $ZnFe_2O_4$ and $CoFe_2O_4$. *Materials Sciences and Applications*, *6*(09), 828.
- Elmustafa, A.A., Stone, S.D.: J. Mech. Phys. Solids. 51; 357–381 (2003)
- Habanjar, K., El Haj Hassan, F. & Awad, R. Comparative studies for the physical properties of superconducting $(BaSnO_3)_x$(Bi, Pb)-2223 samples determined from excess conductivity and thermoelectric power analysis. Mater. Res. Express 6, 096001(2019)
- Hikami, S., Larkin, A.I.: Mod. Phys. Lett. B **2**, 693 (1988)

- Javed, R., Usman, M., Tabassum, S., & Zia, M. (2016). Effect of capping agents: Structural, optical, and biological properties of ZnO nanoparticles. Applied Surface Science; 386:319-326.
- Khadzhai, G. Y., Vovk, N. R., & Vovk, R. V. (2021). Influence of uniform compression on fluctuation paraconductivity of single crystals $Y_{0.77}Pr_{0.23}Ba_2Cu_3O_{7-\delta}$. *Low-Temperature Physics*, *47*(5), 388-391.
- Khan, A., N., Mumtaz, M., Ullah, A., Hassan, N., Khurram, A., A., J. Alloys Compd; **507**
- (2010) 142 .
- Lutterotti, L. (2000). Maud: a Rietveld analysis program designed for the internet and experiment integration. Acta Crystallogr. A, 56, s54.
- Lundqvist, B., Rapp, Ö., Andersson, M.: Phys. Rev. B **62**, 3542 (2000)
- Mohammadizadeh ,M.R., Akhavan M., Physica C **390**, 134 (2003)
- Matsuda, Y., Hirai, T., Komiyama, S.: Solid State Commun. **68**,103 (1988)
- Najjar, R., Awad, R., & Abdel-Gaber, A. M. (2020). Electrical and mechanical properties of Mn_2O_3 nanoparticles/$SmBa_2Cu_3O_{7-\delta}$ composite. *Materials Research Innovations*, *24*(6), 363-372.
- Nasser, A., Srour, A., El Ghouch, N., Malaeb, W., Al-Oweini, R., & Awad, R. (2020). Investigation of the physical properties of $(Cu_{0.5}Tl_{0.5})Ba_2Ca_2Cu_3O_{10-\delta}$ impregnated with mono cobalt (II)-substituted Undecatungstosilicate Nanoparticles. *Applied Physics A*, *126*(12), 1-15.
- Phys, J.A. Activation energy and excess conductivity analysis of $(Ag)_x$ /CuTl-1223 nano-superconductor composites. J. Appl. Phys. 103911, 9 (2014).
- Qasim, Irfan, Waqee-ur-Rehma, M., Mumtaz, M., Hussain, G., Nadeem, K., Shehzad, K., Magn, J., Magn. Mater; **403** (2016) 60
- Rahal, H. T., Abdel-Gaber, A. M., Awad, R., & Abdel-Naby, B. A. (2018). Influence of nitrogen immersion and NiO nanoparticles on the electrochemical behavior of (Bi, Pb)-2223 superconductor in a sodium sulfate solution. *Anti-Corrosion Methods and Materials*.
- Rmeid, S., Basma, H., Roumie, M., Hassan, F. E., & Awad, R. (2019). Vickers Microhardness Studies for $SmBa_2Cu_3O_{7-\delta}$ Added with NiO Nanosized Particles. *Journal of Superconductivity and Novel Magnetism*, *32*(10), 3037-3046.
- Salamati, H., Kameli, P., Solid State Commun; **125** (2003) 407
- Sankar, A., Chitra, S. V., Jayashree, M., Parthibavarman, M., & Anirthavarshini, T. (2022). NiO nanoparticles/graphene nanocomposite as high-performance pseudocapacitor electrodes: Design and implementation. *Diamond and Related Materials*, 108804
- Sery, A. A., Mohamed, W. A., Hammad, F. F., Khalil, M. M., & Farag, H. K. (2022). Synthesis of pure and doped SnO_2 and NiO nanoparticles and evaluation of their photocatalytic activity. *Materials Chemistry and Physics*, *275*, 125190.
- Sun, L., Sun, Y., Fu, Q., & Pan, C. (2021). Facile preparation of NiO nanoparticles anchored on N/P-codoped 3D carbon nanofibers network for high-performance asymmetric supercapacitors. *Journal of Alloys and Compounds*, *888*, 161488.
- Wang, T., Tu, R., Zhang, C., Zhang, S., Wang, K., Goto, T., & Zhang, L. (2021). Influence of oxygen partial pressure on $SmBa_2Cu_3O_{7-\delta}$ film deposited by laser chemical vapor deposition. *Journal of Asian Ceramic Societies*, *9*(1), 197-207.
- Wang, M., Liu, Y., Wang, X., Xian, H., & Yang, W. M. (2021). Influence of Artificially Macroscopical Drilling on the Crystal Growth Orientation of Single Domain SmBCO Bulk Superconductor. *Crystals*, *11*(2), 150.
- Wang, T., Wang, K., Tu, R., Zhang, S., Yang, M., Li, Q., ... & Zhang, L. (2017). Thickness dependence of structure and superconductivity of the $SmBa_2Cu_3O_7$ film by laser CVD. *RSC Advances*, *7*(89), 56166-56172.
- Wen, T.L., Horlin, T., Nygren, M., Mod. Phys; Lett. B **06** (1992) 33.
- White A E, Dynes R C, and Garno J P 1986 *Phys. Rev. B* **33** 3549–52
- White, A. E., Dynes, R. C., & Garno, J. P. (1986). Destruction of superconductivity in quench-condensed two-dimensional films. Physical Review B; 33(5), 3549.
- Zhao, X., Liu, W., Wang, T., Liu, A., Li, T., Chen, Y., ... & Qi, Y. (2021). Growth of $Bi_2Sr_2CaCu_2O_{8+\delta}$ thin films with enhanced superconducting properties by incorporating NiO nanoparticles. *Colloids and Surfaces A: Physicochemical and Engineering Aspects*, *627*, 127121.